

**SHAPE DEPENDENCE OF ELECTRON TRANSFER KINETICS AT
NANOMETER SIZED FILMS****Mariana Chirea^{1*}, Carlos Pereira¹, Fernando Silva¹**

¹Chemistry and Biochemistry Department, Faculty of Sciences, University of Porto, Rua do Campo Alegre 687, 4169-007, Porto, Portugal

Article info**Abstract**

Received: 10.09.2012
Accepted: 16.09.2012
Published: 16.09.2012

Bilayers of gold nanostars (AuNSs) and spherical gold nanoparticles (AuNPs) were fabricated by a self-assembly method based on covalent interactions. 1,5-Pentanedithiol was used as cross-linker molecule for the covalent self-assembly of the nanomaterials on gold electrodes. Electrochemistry of $[Fe(CN)_6]^{3-/4-}$ at the gold nanostar modified electrode reveals charge accumulation and excellent electrocatalytic properties of AuNSs with great sensing potential whereas the redox process at the spherical gold nanoparticles modified electrode reveals an irreversible process.

Keywords | gold nanostars, electrochemical charging, electrocatalytic properties

*Corresponding author e-mail address: mariana.chirea@fc.up.pt

Introduction

The excellent electronic, optical and catalytic properties of nanomaterials are dependent on their shape and size which in turn are responsible for high surface to volume ratio and quantum confinement behavior [1]. Electron transfer at nanoscale is an extremely important process for many applications ranging from optical sensing [2], electrochemical and biochemical sensing [3,4], or fabrication of optoelectronic devices [5,6]. For example, electronic charging of nanoparticles either by chemical injection of electrons using a reductant [7], or electrochemically by applying a potential step [8], results in optical changes of the absorption spectra of metal colloids [8-11]. The correlation of optical and electrochemical properties of nanomaterials helps understand better the sensing properties of nanomaterials. Spectroelectrochemical methods allow a direct correlation between changes in optical spectrum and the number of electrons transferred to nanoparticles when a potential step is applied at an electrode immersed in the nanoparticles' solution [8,9]. For example, Mulvaney et al. have found that the number of electrons transferred at each silver nanoparticle-

electrode encounter was potential dependent and reached 1600 ± 300 at $-0.4V$ vs. Ag/AgCl [8]. The position of surface plasmon band of the silver colloid was blue shifted by 10 nm with an increase of absorbance of about 0.2 revealing electronic charging of the silver sol. A value of $80 \mu F \cdot cm^{-2}$ for the double layer capacitance of the silver nanoparticle-water interface was estimated based on the spectroelectrochemical shift at a 12mM sol concentration [8]. Another approach to study electron transfer at nanoscale is performed by attachment of nanomaterials to the electrodes using various molecular linkers. A wide number of studies [12-19] at nanomaterials modified electrodes have shown that the electron transfer between the electrode and nanomaterials in the presence of various redox probes is rather complex and depends on many parameters [1,12-18] such as size of nanomaterials, [1,12-14] type of ligands at their surface, [15] number of nanomaterials layers, type of outermost layer and presence of pinholes in the film [13,15,16] or lack of pinholes in the film [17]. The electron transfer process was improved by the nanomaterials attached to the

electrodes. The nature of the cross linker molecules has also a strong influence on the overall electron transfer process [19]. Aromatic chain dithiols form electrochemically conductive films whereas aliphatic chain dithiols form electrochemically insulating films [19]. The use of aliphatic chain dithiols as electronic barriers allows a direct evaluation of the nanomaterials' influence in the overall electron transfer process. In this work it is presented the influence of nanomaterials' shape in the electron transfer process. Large gold nanostars and spherical gold nanoparticles were self-

Experiment Details

Chemicals. Hydrogen tetrachloroaurate (III) trihydrate ($\text{HAuCl}_4 \cdot 3\text{H}_2\text{O}$, 99,999 %, Sigma Aldrich), polyvinylpyrrolidone (Fluka, analytical grade, MW 10000 or 40000) sodium borohydride (NaBH_4 , 96%, Sigma Aldrich), N,N-dimethylformamide (DMF, $\geq 99.8\%$, Merck,) 1,5 pentanedithiol, (Aldrich, 96%), potassium hexacyanoferrate (III), potassium hexacyanoferrate (II) (pa quality) and NaClO_4 (pa quality), H_2SO_4 (pure, Pronalab), H_2O_2 30% (Fluka), absolute ethanol and KOH (Sigma Aldrich) were used as received. Millipore filtered water (resistivity $> 18 \text{ M}\Omega \cdot \text{cm}$) was used throughout. Prior use, all the glassware were cleaned with freshly prepared *aqua regia* (HNO_3 : HCl = 1:3, % v/v), rinsed abundantly with Millipore water and dried.

Synthesis of 13.5 nm gold nanoparticles and functionalization with polyvinylpyrrolidone. Gold nanoparticles of 13.5 nm were prepared by standard citrate reduction [21, 22]. Briefly, 5 mL of 1 wt% sodium citrate aqueous solution was added under continuous stirring to a boiling aqueous solution of HAuCl_4 (100 mL, 0.5 mM) and allowed to react for 15 min. Then the solution of colloids was cooled at room temperature and consecutively the AuNPs were transferred into ethanol through PVP functionalization. Thus, 5 mL of a PVP (MW 10 000) aqueous solution, containing a sufficient amount to provide 60 molecules of PVP per nm^2 of gold, was added drop wise to the Au colloid and allowed to react overnight. Finally, it was centrifuged at 4000 rpm for 90 min, the supernatant removed, and the particles redispersed in ethanol. The PVP functionalized AuNPs were used for self-

assembled on 1,5-pentanedithiol modified electrodes. Their surface density was evaluated by scanning electron microscopy (SEM) whereas their electrocatalytic properties were studied by cyclic voltammetry (CV), square wave voltammetry (SQWV) and electrochemical impedance spectroscopy (EIS) using $[\text{Fe}(\text{CN})_6]^{4-/3-}$ as redox probes. It is demonstrated a strong shape effect of the nanomaterials attached to the electrodes with great potential for sensing applications.

assembly on 1,5 pentanedithiol modified electrodes, their electrochemical behavior being evaluated in comparison with the electrochemical behavior of gold nanostars. Also, these AuNPs were used as seeds for the growth of gold nanostars.

Synthesis of Gold Nanostars. In a typical synthesis, 82 μL of an aqueous solution of 50 mM HAuCl_4 was mixed with 15 mL of 10 mM PVP (MW 10 000) solution in DMF [21]. After the complete disappearance of the Au^{3+} CTTS absorption band at 325 nm, a certain amount of preformed-seed dispersion (PVP stabilized AuNPs of 13.20 nm average diameters) was added under continuous stirring and allowed to react until completion of the reaction (no further changes in the UV-Vis-NIR spectra). The ratio of $[\text{HAuCl}_4]$ to $[\text{seed}]$ was 90. The gold nanoparticles and gold nanostars were purified by washing with ethanol (once) and Millipore water (five times) through repeated centrifugation and decantation of the supernatant.

Self-assembly of gold nanostars and spherical gold nanoparticles on gold electrodes. A careful cleaning of the gold electrodes was performed by polishing with diamond suspension (0.3 μm and 0.1 μm), sonication in Millipore water (resistivity $> 18 \text{ M}\Omega \cdot \text{cm}$), electrochemical cycling in aqueous solution of 0.1M HClO_4 between -0.4V to 1.5V, repeated washing with Millipore water and drying. The cleaned gold electrodes were first modified by immersed in 10 mM ethanolic solution of 1, 5 pentanedithiol for 18h overnight. The gold nanostars (1.62×10^9 particles/15mL solution) stabilized with PVP or

spherical gold nanoparticles ($4.23 \times 10^{18}/100\text{mL}$ solution) stabilized with citrate were self-assembled on 1,5-pentanedithiol modified electrodes (Au-1,5PDT-SAM) from aqueous solution during 24h self-assembly time at room temperature (25°C). Cyclic voltammetry, square wave voltammetry and electrochemical impedance spectroscopy measurements were performed on a PGSTAT 302N potentiostat (EcoChemie B.V., The Netherlands) in a standard

three-electrode single compartment cell. A gold electrode of 0.0314 cm^2 area was used as the working electrode. A platinum wire and an Ag/AgCl (3M KCl) electrode were used as counter and reference electrodes, respectively. All the electrochemical measurements were performed in a Faraday cage in order to minimize electrical noise. The electrolyte solution consisted of $0.0005\text{M} [\text{Fe}(\text{CN})_6]^{4-}$, $0.0005\text{M} [\text{Fe}(\text{CN})_6]^{3-}$ and 0.1M NaClO_4 .

Results and Discussions

The average core diameter and tip length of gold nanostars were: $63.50 \pm 0.30\text{ nm}$ and $23.57 \pm 0.52\text{ nm}$ respectively (Figure 1a). The optical spectrum of the gold nanostars shows two surface plasmon bands due to the oscillation of electrons in the conduction band of cores (SPB1 at 550 nm) and tips (SPB2 at 853 nm) (Figure 1b). The spherical gold nanoparticles (AuNPs) were synthesized by citrate reduction²². The average diameter of spherical gold nanoparticles (Figure 1c) was $13.2 \pm 0.04\text{ nm}$ showing one surface plasmon band at 519 nm (Figure 1d) in the optical spectrum. These nanomaterials were self-assembled on 1,5-pentanedithiol modified electrodes through covalent binding. Scanning electron microscopy (SEM) analysis of nanomaterial/dithiol modified electrodes show 45% surface coverage with AuNSs (Figure 2a) and 100% surface coverage with AuNPs (Figure 2e) after 24h self-assembly time. Consecutive cyclic voltammograms (CVs, Figure 2b), square wave voltammograms (SQWVs, Figure 2c) and electrochemical impedance spectroscopy (EIS, Figure 2d) measurements performed at the Au-1,5PDT-AuNS modified electrodes in aqueous solution of $0.5\text{mM} [\text{Fe}(\text{CN})_6]^{3-/4-}$ and 0.1M NaClO_4 demonstrates a transition from slow electron transfer to fast electron transfer. This electrochemical behavior implies a synergic influence of tips and cores in the overall electron transfer process. Initially the CVs and SQWVs show almost no peak currents in the CVs and SQWVs (Fig. 2b, c, blue and pink curves) but consecutive scanning determines an activation of electron transfer process depicted by high current densities with low peak potential separations in the CVs and SQWVs

(orange and green curves, in Fig.2b,c). The evolution of EIS spectra illustrates the same transition from slow to fast electron transfer depicted by the transition from Nyquist diagrams with depressed semicircles and no diffusion profiles (blue and magenta plots in Figure 2d) to Nyquist diagrams with small semicircles at high and intermediated frequency and well defined diffusion profiles (orange and green plots, in Figure 2d). Fittings of the EIS spectra have revealed a strong decrease of charge transfer resistance, R_{CT} , from $189\text{ k}\Omega$ (blue plot, Fig.2d) to $0.55\text{ k}\Omega$ (Fig.2d, green plot) for increasing number of electrochemical measurements (table 1).

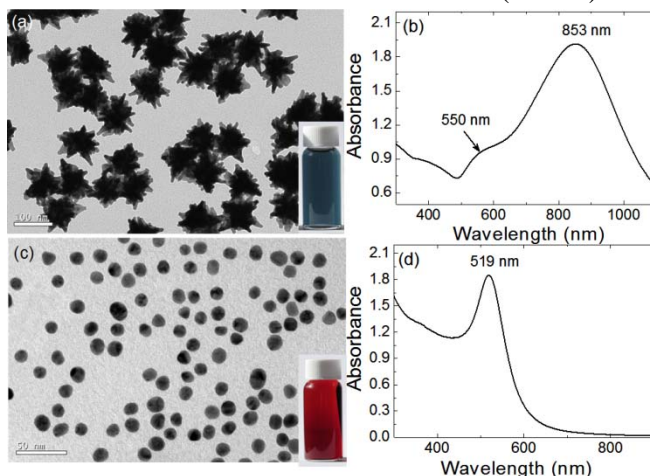


Figure 1: Transmission electron microscopy images and optical spectra of gold nanostars (a, b), and spherical gold nanoparticles (c, d). Inset: photographs of AuNSs solution (blue color) and AuNPs solution (red color).

This decrease of R_{CT} values illustrates a progressive improvement of electron transfer process during continuous exchange of electrons at the AuNS layer. In accordance, the heterogeneous electron transfer constant has drastically increased from $0.89 \times 10^{-7}\text{ cm}^2\text{ s}^{-1}$

¹ (blue plots, Fig.2b, c, d) to $3.04 \times 10^{-5} \text{ cm}^2 \text{ s}^{-1}$ (green plots Fig.2b, c, d). The other parameters obtained from fittings of EIS spectra have revealed additional information concerning the electrochemical properties

of AuNSs assemblies. The capacitance of 1,5PDT-AuNSs bilayer, C_f , has slightly increased (table 1) which could suggest a swelling of the AuNS layer upon diffusion of the probes toward nanostars' surfaces.

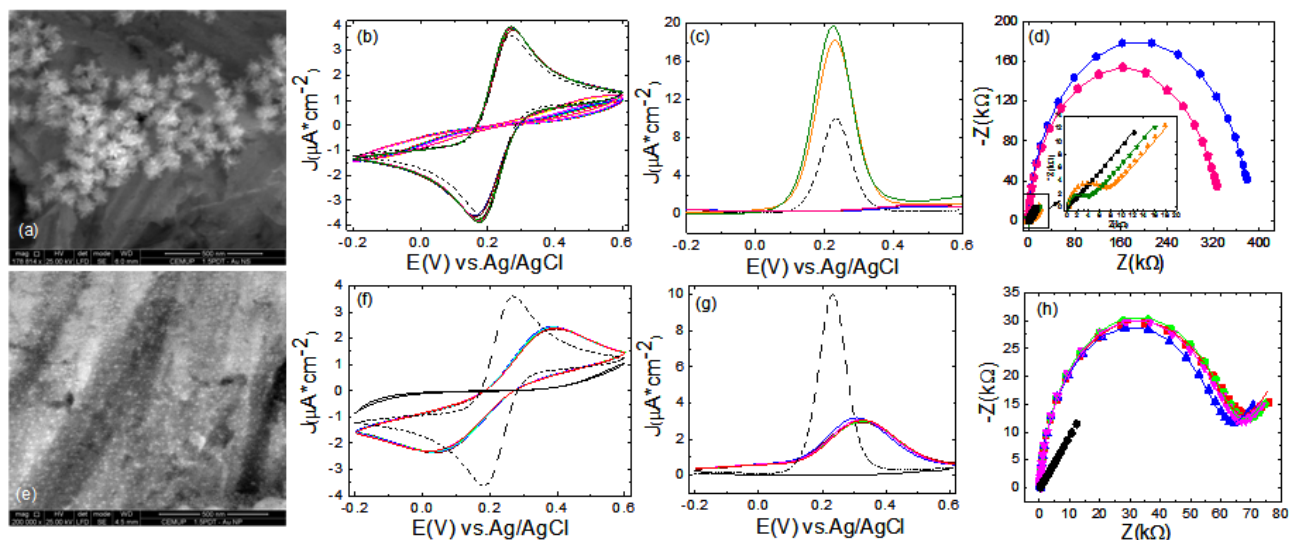


Figure 2: Scanning electron microscopy images of gold nanostars (a) or spherical gold nanoparticles (e) self-assembled on 1,5pentanedithiol modified electrodes. Scale Bar: 500 nm. Consecutive cyclic voltammograms, square wave voltammograms and EIS spectra recorded at the Au-1,5PDT-AuNS modified electrode (b, c, d) and Au-1,5PDT-AuNP modified electrode (f, g, h) in aqueous solution of $0.5 \text{ mM } [\text{Fe}(\text{CN})_6]^{4-/3-}$ and 0.1 M NaClO_4 . Bare gold corresponds to black dashed curves (f, g, h) whereas the Au-1,5PDT-SAM modified electrode corresponds to black straight curves (f, g). EIS spectrum of Au-1,5PDT-SAM modified electrode is presented in Figure 3.

Table 1: Parameter values obtained by fitting the EIS spectra presented in Figures 2d, 2h and 3.

Electrode	R_s (k Ω)	C_f (μF)	R_f (k Ω)	C_{dl} (μF)	R_{CT} (k Ω)
Bare gold	0.287 (0.70)	-	-	1.86 (0.11)	0.61 (0.97)
Au-1,5PDT-SAM	3.52 (0.60)	0.252 (0.48)	2558.4 (0.26)	0.28 (0.92)	2027 (0.97)
Au-1,5PDT-AuNS modified electrode					
EIS plot	R_s (k Ω)	C_f (μF)	R_f (k Ω)	C_{dl} (μF)	R_{CT} (k Ω)
blue	0.327 (0.72)	0.21 (0.60)	171.4 (0.92)	0.08 (0.70)	189.0 (0.97)
magenta	0.330 (0.98)	0.22 (0.58)	120.4 (0.96)	0.10 (0.72)	186.2 (0.42)
orange	0.325 (1.26)	0.63 (0.92)	3.56 (0.96)	4.57 (0.63)	0.65 (0.93)
green	0.326 (0.73)	0.63 (0.80)	3.48 (0.94)	4.60 (0.65)	0.55 (0.90)
Au-1,5PDT-AuNP modified electrode					
EIS plot	R_s (k Ω)	C_f (μF)	R_f (k Ω)	C_{dl} (μF)	R_{CT} (k Ω)
red	0.279 (0.96)	0.39 (0.48)	36.6 (0.72)	0.27 (0.85)	23.17 (0.91)
green	0.283 (0.87)	0.40 (0.56)	37.9 (0.52)	0.42 (0.90)	20.0 (0.79)
magenta	0.283 (0.84)	0.41 (0.80)	38.0 (0.85)	0.30 (0.63)	22.2 (0.85)
blue	0.285 (0.76)	0.40 (0.62)	40.2 (0.96)	0.33 (0.79)	19.5 (0.83)

Values in the brackets represent percent errors for each fit.

SEM analysis of the same electrode before and after electrochemical measurements has revealed similar surface coverage (45%) and no change in shape of AuNSs (results not shown). In consequence, the observed electrochemical behavior is mainly due to the shape of AuNSs. The resistance of the film R_f has decreased two orders of magnitude implying also an improvement of electrical conductivity whereas the double layer capacitance, C_{dl} , has increased about 57 times, from $0.08 \mu\text{F}$ to $4.60 \mu\text{F}$ (table 1) indicating strong charge accumulation at the surface of Au-1,5PDT-AuNS modified electrodes [7]. This charge can be accumulated only on the gold nanostars because no evident increase of double layer capacitance was observed at the bare gold electrode, Au-1,5PDT-SAM or Au-1,5PDT-AuNP modified electrodes (see table 1) during consecutive electrochemical measurements. Compared to spherical gold nanoparticles self-assembled on Au-1,5PDT-SAM modified electrodes (white dots in Figure 2e), the gold nanostars are highly

conductive. The peak currents in the CVs have reached current density of $3.95 \mu\text{A}/\text{cm}^2$ at $\Delta E_p = 0.094\text{V}$ (green curve, Figure 2b) as compared to $2.37 \mu\text{A}/\text{cm}^2$ at $\Delta E_p = 0.330\text{V}$ (blue curve, Figure 2f). Moreover, the electron transfer is faster at Au-1,5PDT-AuNS modified electrodes than at the bare gold electrode itself for which the current density was $3.60 \mu\text{A}/\text{cm}^2$ at $\Delta E_p = 0.086\text{V}$ (black dashed curve, Figure 2f). This high electronic efficiency of gold nanostars is even more evident in the SQWVs for which the current densities reached were $19.75 \mu\text{A}/\text{cm}^2$, at 0.224V (green curve, Figure 2c) as compared to Au-1,5PDT-AuNP modified electrodes (maximum current density $J_a = 3.18 \mu\text{A}/\text{cm}^2$, at 0.305V) or to bare gold (maximum current densities $J_a = 10 \mu\text{A}/\text{cm}^2$ at 0.230V) for the same concentration of redox probes in solution. 1,5Pentanedithiol self-assembled on gold electrodes behaves as a hydrophobic layer restricting the diffusion of the redox probes toward the underlying bare gold electrode and generating voltammograms with no peak currents (straight black lines in Figures 2f and 2g, EIS spectrum is presented in Figure 3). Covalent binding of AuNPs to the Au-1,5PDT-SAM modified electrodes allows a partial recovery of the electronic communication between the redox probes and underlying bare gold electrode. The smaller size of AuNPs usually implies fast electron transfer, [12-14,16,17] but the overall redox process is irreversible at the Au-1,5PDT-AuNP modified electrode (high peak to peak separations in CVs, low current densities in SQWVs and depressed semicircles with no diffusion profiles in EIS spectra, red to blue curves in Fig.2f,g,h). It is evident that the electronic blocking effect of the aliphatic chain dithiol is difficult to overcome despite 100% surface coverage with AuNPs (Fig. 2e). The heterogeneous electron transfer constant was $0.087 \times 10^{-5} \text{ cm} \times \text{s}^{-1}$ (blue curve, Fig.2f,g,h). No evident charging effects were observed at Au-1,5PDT-AuNP modified electrode despite a slight variation of C_{dl} (table 1). All other parameters i.e., R_{CT} , R_f , C_f have remained constant during repeated electrochemical measurements (the EIS spectra have similar features for repeated electrochemical measurements, red to blue Nyquist plots in Figure 2h, table 1). All fittings of EIS spectra were performed using the equivalent electrical circuits presented in

Figure 4. Chis-squared parameter was 10^{-4} magnitude for all fittings yielding confidence bounds of parameters of 98%. In previous reports was demonstrated that the small sized gold nanorods self-assembled to electrodes using similar dithiols can drastically improve the electron transfer process at high surface coverage but no increase of double layer capacitance, C_{dl} , was observed [17]. By comparison, gold nanostars demonstrate high electrical conductivity and charge accumulation effects when self-assembled at insulating Au-1,5PDT-SAM modified electrodes revealing great potential for applications in energy storage devices (i.e. super capacitors) and sensing applications. Due to their high electrical conductivity and high sensitivity to molecular modifications and interactions [23] the gold nanostars are great candidates for electrochemical biosensing applications.

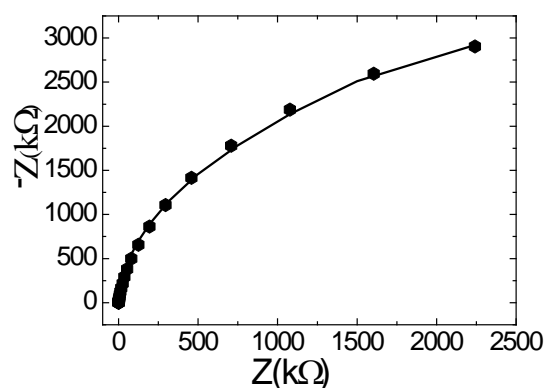


Figure 3: EIS spectrum recorded at Au-1,5PDT-SAM modified electrode in aqueous solution of $0.5\text{mM } [\text{Fe}(\text{CN}_6)]^{3-/4-}$ and 0.1M NaClO_4 . Scattered points represent experimental data, whereas the continuous line represents fitted data.

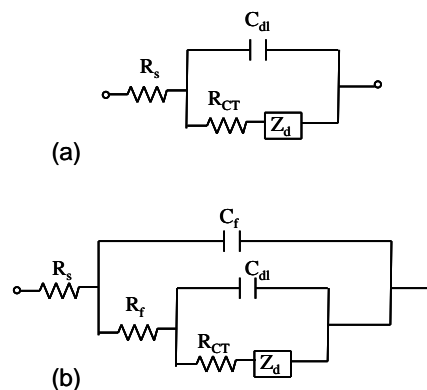


Figure 4: Equivalent electrical circuits used for fitting of impedance spectra in Figures 2(d, h) and 3.

Conclusions

In summary, it was demonstrated that the electron transfer process was shape dependent at isotropic (spherical) and anisotropic (nanostar shaped) gold nanomaterials modified electrodes. Moreover, charge accumulation on a gold nanostar layer was proven by 57 times increase of double layer capacitance, C_{dl} , whereas their excellent electrocatalytic properties were

confirmed by 341 times increase of the heterogeneous electron transfer constant, k_{et} , revealing a great electrochemical sensing potential. The nanostar shaped gold nanoparticles reveal a completely new electrochemical behavior which should be further explored.

Acknowledgments

Financial support from Fundação para a Ciência e a Tecnologia (FCT) of Portugal through the fellowship

SFRH/BPD/39294/2007 is gratefully acknowledged.

References

- [1] D.V. Talapin, J-S. Lee, M.V. Kovalenko, E.V. Shevchenko, Prospects of colloidal nanocrystals for electronic and optoelectronic applications, *Chem. Rev.* 389-458, 110, **2010**.
- [2] M. Moreno, F.M. Ibañez, J.B. Jasinski, F.P. Zamborini, Hydrogen reactivity of palladium nanoparticles coated with mixed monolayers of alkyl thiol and alkyl amines for sensing and catalysis applications *J. Am. Chem. Soc.* 4389-4397, 133, **2011**.
- [3] S.E. Stanca, R. Fitzmaurice, DNA-templated assembly of nanoscale architectures for next-generation electronic devices, *Faraday Discuss.*, 155-165, 131, **2006**.
- [4] Chirea, M., Pereira, E.M., Pereira, C.M., Silva, F., DNA-Biosensor for the detection of actinomycin D, *Biointerface Res. Appl. Chem.*, 151-154, 1(4), **2011**.
- [5] M. Wanunu, R. Popovitz-Biro, H. Cohen, A. Vaskevich, I. Rubinstein, Coordination-based gold nanoparticle layer, *J. Am. Chem. Soc.* 9207-9215, 127, **2005**.
- [6] T. Ung, L.M. Liz-Marzan, P. Mulvaney, Optical properties of thin films of Au@TiO₂ particles, *J. Phys. Chem. B*, 3441-3452, 105, **2001**.
- [7] T. Ung, L.M. Liz-Marzan, P. Mulvaney, Redox catalysis using Ag@SiO₂ colloids, *J. Phys. Chem. B*, 6770-6773, 103, **1999**.
- [8] T. Ung, M. Giersing, D. Dunstan, P. Mulvaney, Spectroelectrochemistry of colloidal silver, *Langmuir*, 1773-1782, 13, **1997**.
- [9] R. Chapman, P. Mulvaney, Electro-optical shifts in silver nanoparticle films, *Chem. Phys. Lett.*, 358-362, **2001**.
- [10] Mulvaney, P. In *Electrochemistry of Colloids and Dispersions*; Mackay, R. A., Texter, J., Eds.; VCH: New York, 345, **1992**.
- [11] A. Henglein, P. Mulvaney, T. Linnert, Chemistry of Ag_n aggregates in aqueous solution: non-metallic oligomeric clusters and metallic particles, *Faraday Discuss.*, 31-34, 92, **1991**.
- [12] M. Chirea, A. Cruz, C.M. Pereira, A.F. Silva, Size-dependent electrochemical properties of gold nanorods, *J. Phys. Chem. C*, 13077-13087, 113, **2009**.
- [13] M. Chirea, C.M. Pereira, F. Silva, Catalytic effect of gold nanoparticles self-assembled in multilayered polyelectrolyte films, *J. Phys. Chem. C.*, 9255-9266, 111, **2007**.
- [14] M. Chirea, E.M. Pereira, C-M. Pereira, F. Silva, Synthesis of poly-Lysine/gold nanoparticles films and their electrocatalytic properties, *Biointerface Res. Appl. Chem.*, 1(4), 119-126, **2011**.
- [15] M. Chirea, V. García-Morales, J.A. Manzanares, C. Pereira, R. Gulaboski, F. Silva, Electrochemical characterization of polyelectrolyte/gold nanoparticle multilayers self-assembled on gold electrodes, *J. Phys. Chem. B*, 109, 21808-21817, **2005**.
- [16] M. Chirea, C. Pereira, F. Silva chapter 7 in *Nanorods*, Intech, Croatia, 129, **2012**.
- [17] M. Chirea, J. Borges, C.M. Pereira, F. Silva, Density dependent electrochemical properties of vertically aligned gold nanorods, *J. Phys. Chem. C*, 114, 9478-9488, **2010**.
- [18] J.F. Hicks, F.P. Zamborini, R.W. Murray, Dynamics of electron transfers between electrodes and monolayers of nanoparticles, *J. Phys. Chem. B.*, 106, 7751-7757, **2002**.
- [19] S.L. Horswell, I.A. O'Neil, D.J. Schiffrin, Kinetics of electron transfer at Pt nanostructured film electrodes, *J. Phys. Chem. B*, 107, 4844-4854, **2003**.
- [20] C. Love, L.A. Estroff, J.K. Kriebel, R.G. Nuzzo, Whitesides G. M. Self-assembled monolayers of thiolates as a form of nanotechnology, *Chem. Rev.*, 105, 1103-1170, **2005**.
- [21] S. Barbosa, A. Agrawal, L. Rodriguez-Lorenzo, I. Pastoriza-Santos, R. A. Alvarez-Puebla, A. Kornowski, H. Weller, L. M. Liz-Marzan, Tuning size and sensing properties in colloidal gold nanostars, *Langmuir*, 26, 14943-14950, **2010**.
- [22] B.V. Enustun, J. Turkevich, Coagulation of colloidal gold, *J. Am. Chem. Soc.*, 85, 3317-3328, **1963**.
- [23] S.K. Dondapati, T.K. Sau, C. Hrelescu, T.A. Klar, F.D. Stefani, J. Feldmann, Label-free biosensing based on single gold nanostars as plasmonic transducers, *ACS Nano*, 4,(11), 6318-6322, **2010**.